

Article

A Study of the Optical Properties and Fabrication of Coatings Made of Three-Dimensional Photonic Glass

Chih-Ling Huang 

Center for Fundamental Science, Kaohsiung Medical University, Kaohsiung 807, Taiwan; chihling@kmu.edu.tw;
Tel.: +886-7-312-1101

Received: 30 June 2020; Accepted: 11 August 2020; Published: 12 August 2020



Abstract: Photonic crystals employ optical properties based on optical, physical, chemical, and material science. Nanosilica particles have a high specific surface area and are widely used in nanotechnology research and biomedical applications. In this study, nanosilica particles were fabricated by sol–gel methods, and the particle sizes of the silica nanoparticles were 280, 232, and 187 nm, based on dynamic light scattering. The silica nanoparticle suspension solution was heated to boiling for fast evaporation processing for self-assembly to fabricate three-dimensional photonic glass for structural color coatings. The sample had an adjustable structural color (red: 640 nm, green: 532 nm, and blue: 432 nm). The microstructures of various structure-colored samples were arranged, but there was a disordered solid arrangement of silica nanoparticles. These were not perfect opal-based photonic crystals. Compared to opal-based photonic crystals, the arrangement of silica nanoparticles was a glassy structure with a short-range order. Due to the accumulation of silica nanoparticle aggregates, samples displayed a stable colloidal film, independent of the viewing angle. In our study, the fast solvent evaporation in the self-assembly process led to the formation of a colloidal amorphous array, and it fitted the requirement for non-iridescence. Non-iridescent photonic glass with various colors was obtained. This type of color coating has wide potential applications, including reflective displays, colorimetric sensors, textiles, and buildings.

Keywords: photonic crystal; photonic glass; self-assembly; silica; sol–gel; structure-color

1. Introduction

A variety of natural creatures are of research interest. With the development of nanotechnology, scientists have found that color comes from chemical dye molecules and physical structural color. Dye pigment can selectively absorb the light of different wavelengths [1] and reflect the light of a specific wavelength so that the object exhibits different colors. Dye molecules with different chemical structures can be adjusted to produce different colors and fluorescent properties [2]. However, dye pigment molecules are susceptible to fading and discoloration due to various factors (such as light, temperature, oxidation, pH) [3]. The physical structural color is completely different from the dye pigment. It is the result of optical effects, such as interference, diffraction, and scattering of the structures [4]. For example, regarding the colorful and striking brilliancy feathers of the peacock tail, the color is due to feathers containing two-dimensional (2D) photonic-crystal structures [5]. Additionally, the male of the *Hoplia coerulea* beetle shows a blue-violet color due to the beetle's cuticle covered by scales [6]. Moreover, morpho butterflies exhibit surprisingly brilliant blue wings originating from the submicron structure created on the scales of the wing [7].

In nature, some species, such as chameleons, have physical structural colors. They can change their skin color arbitrarily. In the past, the effect of discoloration was generally considered to be achieved by regulating the distribution of pigment molecules in skin tissue. In recent years, it has been found that the skin tissue of the chameleon contains nano-sized crystals. The periodically arranged crystals

form periodic structures and can change the period of the nanocrystal arrangement by shrinking or relaxing the skin tissue. The refracted light of the epidermis of chameleons is modulated arbitrarily by the results of physics [8]. The advantage of physical structural color is that it depends on the periodic size, arrangement, and dielectric constant of the materials in photonic crystals. There is no defect of fading or failure caused by dye pigment decomposition.

Photonic crystals are periodic structures formed by dielectric materials, and these special structures are repeatedly arranged to form solid crystals [9]. When light passes through a three-dimensional (3D) photonic crystal, the intensity of the electromagnetic wave in a specific wavelength band is greatly reduced due to destructive interference. Incident light of a specific wavelength cannot be transmitted inside the structure and form a photonic energy gap. This physical phenomenon is the basis of structural color. Coatings are made via self-assembly methods and can be used as surface-enhanced Raman scattering substrates. When the crystals exhibit various structural colors, the wavelength of the reflected light increases as the particle size increases. When the photonic band gap overlaps the wavelength of the incident laser source for the Raman spectrum, surface-enhanced Raman scattering is significantly enhanced [10]. Based on their optical properties, the coatings have potential in various fields, such as biomimetic fabrication, surface-enhanced Raman scattering, and other biological or electronic applications.

Polystyrene has a unique dielectric property and good dimensional control. It is a commonly used material for making photonic crystals [11]. In a previous study, the synthesis of polystyrene particles was conducted via emulsification and a self-assembly process. It is an opal crystal array and can be developed as a rapid qualitative detection device for methanol and ethanol. However, polystyrene is a thermoplastic polymer material, and its glass transition temperature is about 80–90 °C. It is not suitable for use in a high-temperature environment and has a poor chemical stability. It is easily corroded by acid, alkali, and various organic solvents and is discolored by exposure to ultraviolet light. These disadvantages make it poor for application in outdoor or acid–base environments.

Silica is a stable material and widely used in sensors [12], optoelectronics [13], quantum devices [14], environmental science [15], and biomaterials [16]. Compared to organic polymer materials such as polystyrene, silica is an inorganic material, which can be applied in a wider range of applications. Silica is not limited by the poor tolerance of polymer materials, and can be used in high-temperature or acid–base environments [17]. In this study, silica nanospheres with various diameters were fabricated and self-assembly-arranged to form the structural color coating.

2. Materials and Methods

In this study, we used the sol–gel method and tetraethoxysilane (TEOS) as the precursor to fabricate silica nanoparticles via their condensation and a hydrolysis reaction [18]. Silica (SiO₂, i.e., transparent material in normal glass) was used, but not silicon (Si, an opaque material with a large absorption in the visible region). In an acid environment, the reaction rate of hydrolysis was higher than the reaction rate of condensation. The particle size was very small, but increased as the pH value increased. Sample color changing was tuned by photonic crystals, by varying the period or size of the nanospheres. The amount of precursor also influenced the particle size. Adding ethanol slowed down the rate of the hydrolysis reaction and adding TEOS was the main factor in the size increase. The preparation methods were described in our previous study [19], and the formula is given in Table 1.

Table 1. Precursor quantities of silica nanoparticle fabrication used to produce various structural color samples.

Sample Color	NH ₄ OH (mL)	H ₂ O (mL)	TEOS (mL)	Ethanol (mL)
Blue	1	9	1	9
Green	3	7	1	9
Red	5	5	1	9

Photonic crystals with structural color were formed by self-assembly arrangement as periodic structures [20]. Silica colloidal crystal coatings were prepared via self-assembly, which was forced by solvent evaporation. A glass slide was used as the substrate. Samples were placed in beakers that contained a silica nanoparticle suspension solution, and the solution was then heated to boiling. This led to fast evaporation processing. The solvent was stirred and evaporated, and the silica nanoparticles were anchored and remained upon the sample surface, and arranged via self-assembly.

The color of the samples was analyzed by the transmittance of the sample at different wavelengths. It was obtained by an ultraviolet-visible spectrophotometer (UV-VIS, U4100, HITACHI, Tokyo, Japan). Field-emission scanning electron microscopy (FE-SEM, AURIGA, ZEISS, Oberkochen, Germany) with a Schottky emitter was used to observe the microstructures of samples. A transmission electron microscope (TEM, JEM-1400, JEOL, Tokyo, Japan) was used to observe the silica nanoparticles. Dynamic light scattering (DLS, Delsa Nano C, Beckman Coulter, Brea, CA, USA) was used to analyze the diameter and polydispersity index (PDI) of the silica nanoparticles.

3. Results and Discussion

By adjusting the concentration of the reaction precursor, the ratio of water and ethanol, and the pH, appropriate particle sizes can be screened [19]. The sample was prepared by stacking the silica nanoparticles by self-assembly, as shown in Figure 1. The sol-gel method was used to prepare the silica matrix nanospheres, which were stacked into 3D structures with red, green, and blue structural colors by self-assembly, which was affected by the structure, diffraction, and scattering. As a result of the optical effect, the color was completely different from the dye pigment molecule. Based on the Bragg reflection, the specific wavelength became brighter and the other wavelengths became darker, so the sample emitted a bright color [21].



Figure 1. Silica-based photonic glass with various colors.

The advantages of using the sol-gel method to prepare nanomaterials are the low synthesis temperature; large vacuum process equipment; adjustable composition ratio; organic and inorganic doping; and uniformity of the particle size, controlled to obtain a high purity. The uniformity of the sample was very high. The sol-gel method uses a chemically active compound as a precursor, and the reactant and precursor are uniformly dispersed in a liquid phase environment. The solution is gradually formed into a sol system by temperature, concentration, pH, etc., and colloidal particles are formed. They gradually aggregate and form a polymeric structure to produce a three-dimensional gel structure. When the solvent in the voids of the gel framework is volatilized and dried, a material with a nanostructure can be prepared [18]. This means that silica nanospheres of different particle sizes

can be prepared, and the nanospheres of different particle sizes can correspond to different reflection wavelengths, so that the samples exhibit different structural colors.

The transmittance of the sample at different wavelengths was obtained by an ultraviolet-visible spectrophotometer (UV-VIS). As shown in Figure 2, the corresponding reflection wavelengths of the three-color samples were 432, 532, and 640 nm, respectively. The red line is the spectrum of the sample with a red color, so we marked the minimum transmission at 640 nm in the red color region (600–700 nm). The minimum transmission was also found at the wavelength of 380 nm, but it was in the UV region and was not marked. Sharp changes in transmission were observed for all three lines at 700 nm. The ultraviolet-visible spectrophotometer (UV-VIS, HITACHI U4100, Tokyo, Japan) has dual detectors, and the detector change wavelength can be set at 700–900 nm. In this study, the detector change wavelength was set at 700 nm because the visible-light region was 400–700 nm. The wavelength range of visible light is 400–700 nm. The common blue wavelength is 450 nm, the green wavelength is 540 nm, and the red wavelength is 633 nm. The differences between the reflection wavelengths of the samples prepared in this study were 18, 8, and 7 nm.

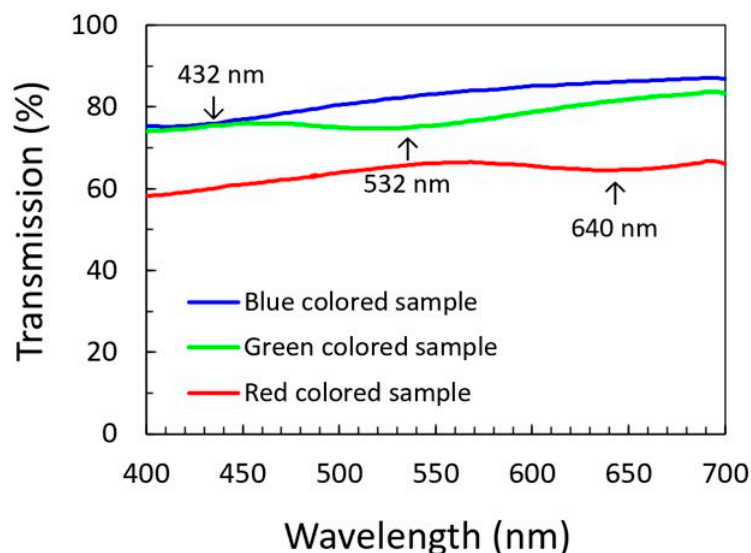


Figure 2. Transmission spectrum for visible light of various colored samples.

Nanosilica particles of various sizes were fabricated via various conditions by tuning the amount of NH_4OH . In Table 1, these three conditions correspond to various colors (shown in Figure 1). The minimum transmission (shown in Figure 2) was marked and used to determine the relationship with the particle size. Due to the various fabrication conditions, the coatings could be made by opal-based photonic crystals, vacancy-doped photonic crystals, and photonic glass [22–25]. The real samples produced by self-assembly via various conditions were what we presented for the scientific and technical information as a promising strategy for coatings.

The silica nanoparticles were stacked into a three-dimensional structure by self-assembly. The sample was observed by SEM and is shown in Figure 3. The silica nanoparticles were observed by TEM and are shown in Figure 4. The silica nanoparticles had a uniform spherical shape, and the size ranged from 200 to 400 nm. This shows that the particles were closely arranged and had a multi-layer structure. When the photonic crystal sample was self-assembled and formed, the defects or vacancies meant that the structures were not tightly packed. The volume fraction of the photonic crystal was decreased, and this caused the equivalent refractive index to decrease. This led to a blue shift in the reflected light.

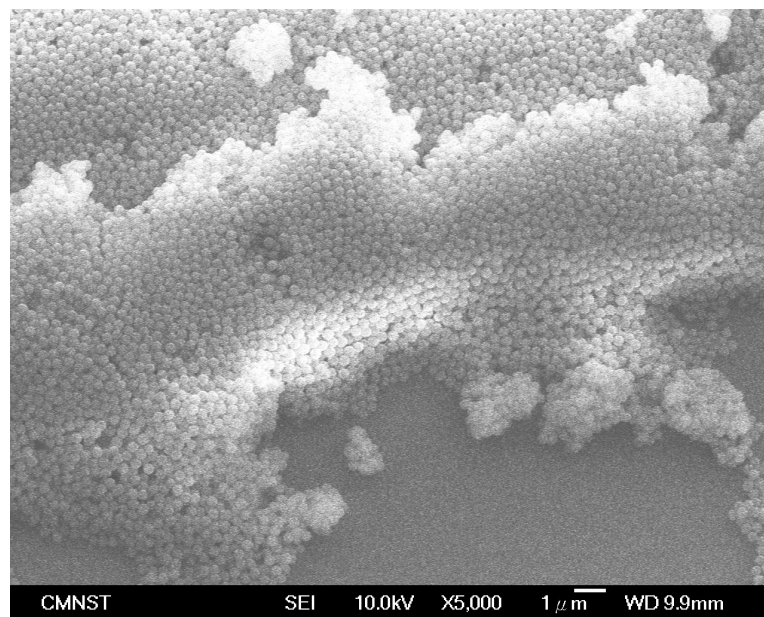


Figure 3. Three-dimensional structure produced by silica nanoparticles observed by SEM.

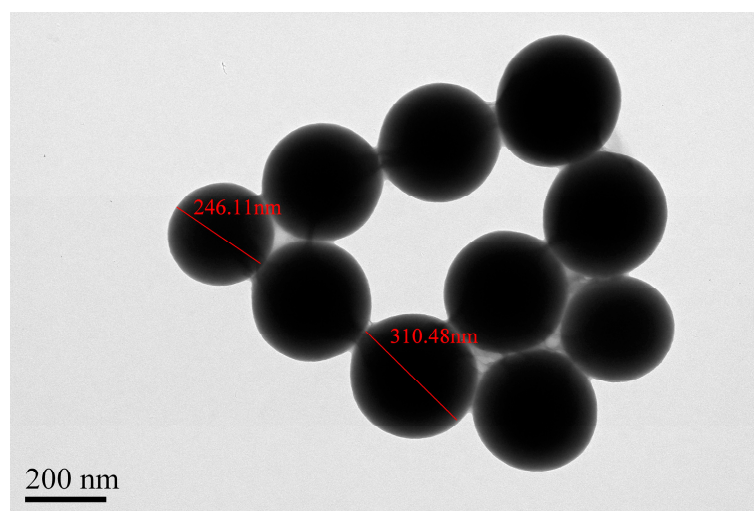


Figure 4. Silica nanoparticles observed by TEM.

According to Bragg's law [26], the photonic crystal energy gap can be calculated. The diffraction wavelength λ can be calculated by the plane spacing d_{hkl} of the crystal plane (hkl), the incident angle θ , and the equivalent refractive index n_{eff} , as shown in Equation (1). The photonic crystal can be regarded as a uniform medium, and the dispersive medium can calculate the equivalent refractive index n_{eff} as Equation (2) [27]:

$$\lambda = 2d_{hkl} \left[n_{\text{eff}}^2 - \sin^2 \theta \right]^{\frac{1}{2}} \quad (1)$$

$$n_{\text{eff}}^2 = \left[n_p f_p + n_{\text{air}} (1 - f_p) \right]^2 \quad (2)$$

where n_p and n_{air} are the refractive indices of the photonic crystal and air, and the volume fraction of the photonic crystal is f_p . According to the calculation results, the crystals were arranged in a body-centered cubic (BCC) crystal structure with a volume fraction of 0.68; if the crystal was arranged in a face-centered cubic (FCC) crystal structure, the volume fraction was 0.74, and if the crystal was arranged in a hexagonal close-packed (HCP) crystal structure, the volume fraction was also 0.74. For example, in the densely packed state, the equivalent refractive index of the silica photonic crystal

was calculated by FCC ($f_p = 0.74$), the refractive index n_{air} of the air was 1, and the refractive index n_p of the silica photonic crystal was 1.5. The equivalent refractive index n_{eff} of the silica photonic crystal was 1.37. The lattice constant a of the FCC structure was calculated from the accumulated atomic diameter D by $a^2 + a^2 = (2D)^2$, and the plane spacing d_{hkl} of the crystal plane (hkl) was calculated as follows:

$$d_{hkl}^2 = \frac{a^2}{(h^2 + k^2 + l^2)}. \quad (3)$$

The (111) plane spacing of the FCC structure was $d_{111} = 0.816 D$. If the incident angle is 0° , and the equivalent refractive index n_{eff} of the silica photonic crystal is 1.37, the wavelength of the reflected light of the photonic crystal is $\lambda = 2.236 D$. In this study, the silica nanoparticles had a uniform spherical structure with a size ranging from about 200 to 400 nm. The above theory could be used to estimate the wavelength range of the reflected light from 447 to 894 nm and in the visible wavelength, so the samples had structural colors corresponding to reflected light in the range of visible light.

The size of silica nanoparticles prepared by different conditions was measured by DLS. The polydispersity index (PDI) values of the silica nanoparticles were 0.139 ± 0.010 , 0.203 ± 0.017 , and 0.189 ± 0.010 for blue, green, and red samples, respectively. The PDI values ranged from 0.0 (for a perfectly uniform sample) to 1.0 (for a highly polydisperse sample). Values of 0.2 or below were deemed acceptable and suggested that the particles had narrow size distributions and were largely homogeneous [28,29]. The sizes of the silica nanoparticles were 258 ± 9 , 303 ± 6 , and 389 ± 20 nm for blue, green, and red samples, respectively.

The DLS measurement results are shown in Figure 5. DLS detects the size of the silica nanoparticle, and the measured particle size is a range. It was found that the nanoparticle easily formed micron-scale clusters such that the particle size measurement value was too high. In order to correct the measured particle size, the measured value of the reflected wavelength was calculated by the formula, the particle size was calculated, and the energy distribution and quantity distribution of the sample were measured with a dynamic laser light scattering instrument. The particle diameters obtained by the volume distribution were compared, and the results are shown in Table 2.

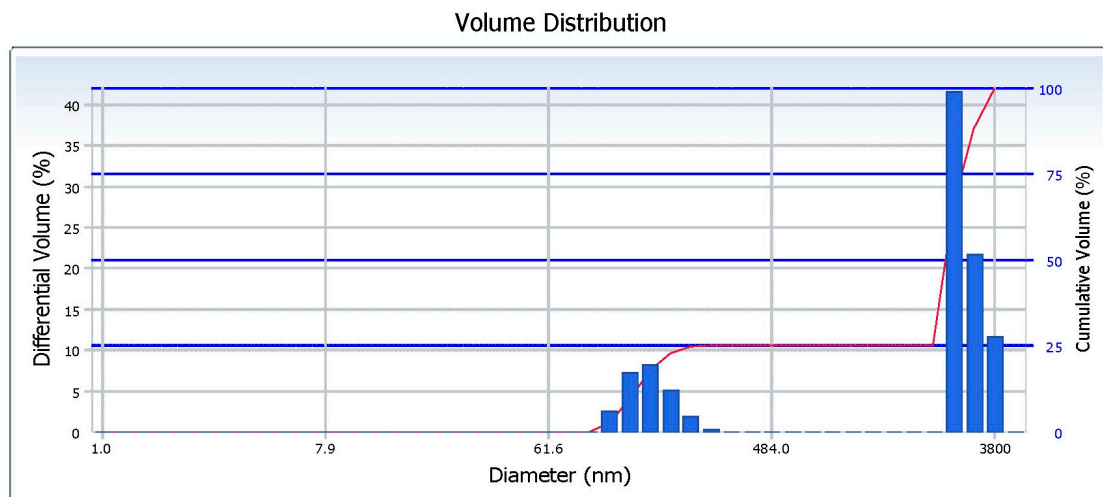


Figure 5. Silica particle diameter measured by dynamic light scattering (DLS).

Table 2. The sample color and various diameters of silica nanoparticles of samples.

Sample Color	Calculated Diameter (nm)	Intensity Distribution Diameter (nm)	Number Distribution Diameter (nm)	Volume Distribution Diameter (nm)
Blue	193	187 ± 8	145 ± 6	163 ± 6
Green	238	296 ± 17	186 ± 35	231 ± 16
Red	286	280 ± 3	288 ± 15	251 ± 10

As the particle size measured by DLS was not the true size of the nanoparticle but was the hydraulic diameter of the nanoparticle in the solution, the dimensional data directly observed by the TEM was higher. The DLS-measured results obtained by the illuminating scatter meter were calculated by measuring the light intensity; therefore, the value obtained by the intensity distribution was closer to the true size. As shown in Table 2, the particle sizes obtained by the intensity distribution were 187 ± 8, 296 ± 17, and 280 ± 3 nm, respectively, compared to the values calculated by the formula, which were 193, 238, and 286 nm, and the error was 3%, 24%, and 2%, respectively. The standard deviation and error of the blue and red-light samples were quite small. The particle size measurement obtained by the energy distribution was similar to the calculated value of the sample, but the color of the light was green. The standard deviation and error of the light sample were large. Therefore, the value of the number distribution was required. The particle size of the green light sample after normalization was 232 nm, and the formula was calculated. The error was 3% with respect to 238 nm. Through the measurement of the particle size, the calculated wavelength of the reflected light of the samples was recalculated, and the wavelength of the measured value and the calculated value of the wavelength were compared to obtain the blue-shift wavelength, the color of the reflected light of different samples, and the wavelength. The measured value, the calculated wavelength value, and the blue-shift wavelength are shown in Table 3. The sample did not consist of opal-based photonic crystals, but possibly vacancy-doped photonic crystals or photonic glass. Short-term or long-term ordering structures still exist. According to Bragg–Snell’s law, the calculated wavelengths of the three samples are 418, 519, and 626 nm, respectively. Compared to the theoretical calculations, the variety between measured values and calculated wavelengths are within 15 nm. Therefore, the normal incidence angle in Equation (1) helps us to explain the basic wavelength of structural color.

Table 3. The measured and calculated wavelengths of samples with various colors.

Sample Color	Measured Wavelength (nm)	Calculated Wavelength (nm)	Blue Shift (nm)
Blue	432	418	14
Green	532	519	13
Red	640	626	14

Moreover, the sample did not consist of opal-based photonic crystals, but possibly vacancy-doped photonic crystals or photonic glass. In order to observe the lack of ordering, the microstructures of various structure-colored samples were observed and enlarged, as shown in Figure 6. The microstructures were arranged, but there was a disordered solid arrangement of silica nanoparticles. These were not perfect opal-based photonic crystals. Compared to the opal-based photonic crystals, the silica nanoparticles formed a glassy structure with a short-range order. Non-iridescent structural colors based on a disordered arrangement of monodisperse spherical particles, also called photonic glass, show low color saturation due to a gradual transition in the reflectivity spectrum [24]. Due to the accumulation of silica nanoparticle aggregates, samples showed a stable colloidal film, independent of the viewing angle [30]. In our study, the fast solvent evaporation in the self-assembly process led to the formation of a colloidal amorphous array, and it met the requirement for non-iridescence (shown in Figure 7). Non-iridescent photonic glass with various colors was obtained. This type of color coating has wide potential applications, including in reflective displays [31], colorimetric sensors [32], textiles [33], and buildings [34].

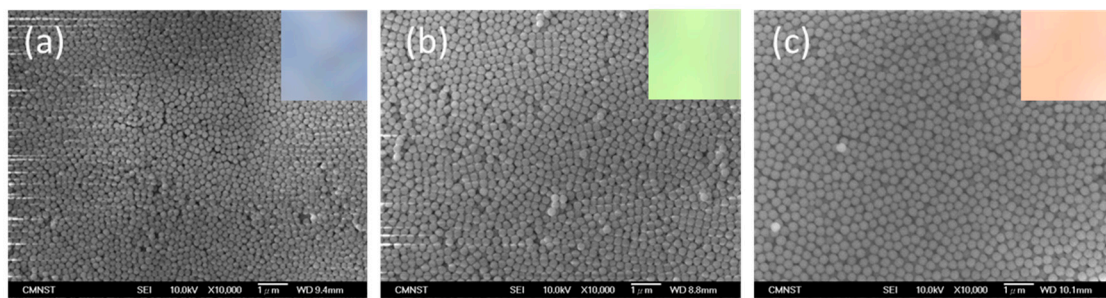


Figure 6. Microstructures of various structure-colored samples: (a) Blue, (b) green, and (c) red. Sample color is shown in the corner of each image.

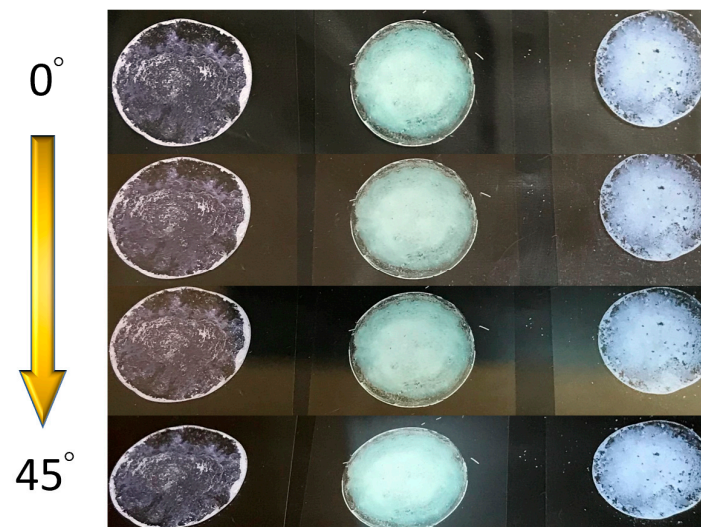


Figure 7. The photographs at various incident angles (0° – 45°) for different nanoparticle sizes.

4. Conclusions

In this study, nanosilica particles were fabricated by sol–gel methods, and the particle sizes of the silica nanoparticles were controlled by tuning the amount of NH_4OH . The silica nanoparticle sizes were 280, 232, and 187 nm, based on dynamic light scattering. The silica nanoparticle suspension solution was heated to boiling for fast evaporation processing for self-assembly to fabricate three-dimensional photonic glass for structural color coatings. The sample had an adjustable structural color (red: 640 nm, green: 532 nm, and blue: 432 nm). Compared to the opal-based photonic crystal, the arrangement of silica nanoparticles was a glassy structure with a short-range order. Due to the accumulation of silica nanoparticle aggregates, samples displayed a stable colloidal film, independent of the viewing angle. The fast solvent evaporation in the self-assembly process led to the formation of a colloidal amorphous array, and it fitted the requirement for non-iridescence. Non-iridescent photonic glass with various colors was obtained in this study. This type of color coating has wide potential applications, including reflective displays, colorimetric sensors, textiles, and buildings.

Funding: This research was funded by the Ministry of Science and Technology (MOST) in Taiwan, grant number MOST-106-2221-E-037-004 and MOST 108-2221-E-037-001-MY2.

Conflicts of Interest: The author declares that there are no conflict of interest.

References

1. Wang, L.; Zhang, P.; Shi, J.; Hao, Y.; Meng, D.; Zhao, Y.; Yanyan, Y.; Li, D.; Chang, J.; Zhang, Z. Radiofrequency-triggered tumor-targeting delivery system for theranostics application. *ACS Appl. Mater. Interfaces* **2015**, *7*, 5736–5747. [[CrossRef](#)] [[PubMed](#)]
2. Owens, G.J.; Singh, R.K.; Foroutan, F.; Alqaysi, M.; Han, C.-M.; Mahapatra, C.; Kim, H.-W.; Knowles, J.C. Sol–gel based materials for biomedical applications. *Prog. Mater. Sci.* **2016**, *77*, 1–79. [[CrossRef](#)]
3. Kan, C.-w.; Cheung, H.-f.; Chan, Q. A study of plasma-induced ozone treatment on the colour fading of dyed cotton. *J. Clean. Prod.* **2016**, *112*, 3514–3524. [[CrossRef](#)]
4. Liu, G.; Zhou, L.; Zhang, G.; Li, Y.; Chai, L.; Fan, Q.; Shao, J. Fabrication of patterned photonic crystals with brilliant structural colors on fabric substrates using ink-jet printing technology. *Mater. Des.* **2017**, *114*, 10–17. [[CrossRef](#)]
5. Jiang, Y.; Wang, R.; Feng, L.; Zhang, D. Mechanochromic response of the barbules in peacock tail feather. *Opt. Mater.* **2018**, *75*, 74–78. [[CrossRef](#)]
6. Vigneron, J.P.; Colomer, J.-F.; Vigneron, N.; Lousse, V. Natural layer-by-layer photonic structure in the squamae of *Hoplia coerulea* (Coleoptera). *Phys. Rev. E* **2005**, *72*, 061904. [[CrossRef](#)] [[PubMed](#)]
7. Kinoshita, S.; Yoshioka, S.; Fujii, Y.; Okamoto, N. Photophysics of structural color in the Morpho butterflies. *Forma* **2002**, *17*, 103–121.
8. Teyssier, J.; Saenko, S.V.; van der Marel, D.; Milinkovitch, M.C. Photonic crystals cause active colour change in chameleons. *Nat. Commun.* **2015**, *6*, 6368. [[CrossRef](#)]
9. Yablonovitch, E. Inhibited spontaneous emission in solid-state physics and electronics. *Phys. Rev. Lett.* **1987**, *58*, 2059–2062. [[CrossRef](#)]
10. Ye, X.; Qi, L. Two-dimensionally patterned nanostructures based on monolayer colloidal crystals: Controllable fabrication, assembly, and applications. *Nano Today* **2011**, *6*, 608–631. [[CrossRef](#)]
11. Kuo, W.-K.; Weng, H.-P.; Hsu, J.-J.; Yu, H.H. A bioinspired color-changing polystyrene microarray as a rapid qualitative sensor for methanol and ethanol. *Mater. Chem. Phys.* **2016**, *173*, 285–290. [[CrossRef](#)]
12. Pi, M.; Zheng, C.; Bi, R.; Zhao, H.; Liang, L.; Zhang, Y.; Wang, Y.; Tittel, F.K. Design of a mid-infrared suspended chalcogenide/silica-on-silicon slot-waveguide spectroscopic gas sensor with enhanced light-gas interaction effect. *Sens. Actuators B: Chem.* **2019**, *297*, 126732. [[CrossRef](#)]
13. Omri, K.; Lahouli, R.; El Mir, L. Microstructure and electrical properties of silica–Zn₂SiO₄–Mn glass-ceramics as composite for optoelectronic devices. *Results Phys.* **2019**, *12*, 2141–2145. [[CrossRef](#)]
14. Song, W.-S.; Kim, J.-H.; Yang, H. Silica-embedded quantum dots as downconverters of light-emitting diode and effect of silica on device operational stability. *Mater. Lett.* **2013**, *111*, 104–107. [[CrossRef](#)]
15. Yazdanpanah, M.; Nojavan, S. Polydopamine-assisted attachment of β -cyclodextrin onto iron oxide/silica core-shell nanoparticles for magnetic dispersive solid phase extraction of aromatic molecules from environmental water samples. *J. Chromatogr. A* **2019**, *1601*, 9–20. [[CrossRef](#)] [[PubMed](#)]
16. El-Hamid, H.K.A.; Radwan, M.M. Influence of nano-silica additions on hydration characteristics and cytotoxicity of calcium aluminate as biomaterial. *Heliyon* **2019**, *5*, e02135. [[CrossRef](#)]
17. Das, S.; Saha, B.; Bhaumik, S. Experimental study of nucleate pool boiling heat transfer of water by surface functionalization with SiO₂ nanostructure. *Exp. Therm. Fluid Sci.* **2017**, *81*, 454–465. [[CrossRef](#)]
18. Perullini, M.; Calcabrini, M.; Jobbágy, M.; Bilmes Sara, A. Alginate/porous silica matrices for the encapsulation of living organisms: Tunable properties for biosensors, modular bioreactors, and bioremediation devices. *Open Mater. Sci.* **2019**, *1*, 3–12. [[CrossRef](#)]
19. Huang, C.-L.; Fang, W.; Chen, I.H.; Hung, T.-Y. Manufacture and biomimetic mineral deposition of nanoscale bioactive glasses with mesoporous structures using sol-gel methods. *Ceram. Int.* **2018**, *44*, 17224–17229. [[CrossRef](#)]
20. Miklyae, V.V.; Meisel, D.C.; Blanco, A.; von Freymann, G.; Busch, K.; Koch, W.; Enkrich, C.; Deubel, M.; Wegener, M. Three-dimensional face-centered-cubic photonic crystal templates by laser holography: Fabrication, optical characterization, and band-structure calculations. *Appl. Phys. Lett.* **2003**, *82*, 1284–1286. [[CrossRef](#)]
21. Shi, X.; He, J.; Xie, X.; Dou, R.; Lu, X. Photonic crystals with vivid structure color and robust mechanical strength. *Dye. Pigment.* **2019**, *165*, 137–143. [[CrossRef](#)]

22. García, P.D.; Sapienza, R.; Blanco, Á.; López, C. Photonic glass: A novel random material for light. *Adv. Mater.* **2007**, *19*, 2597–2602. [[CrossRef](#)]
23. García, P.D.; Sapienza, R.; López, C. Photonic glasses: A step beyond white paint. *Adv. Mater.* **2010**, *22*, 12–19. [[CrossRef](#)] [[PubMed](#)]
24. Shang, G.; Maiwald, L.; Renner, H.; Jalas, D.; Dosta, M.; Heinrich, S.; Petrov, A.; Eich, M. Photonic glass for high contrast structural color. *Sci. Rep.* **2018**, *8*, 7804. [[CrossRef](#)] [[PubMed](#)]
25. Schertel, L.; Wimmer, I.; Besirskic, P.; Aegerter, C.M.; Maret, G.; Polarz, S.; Aubry, G.J. Tunable high-index photonic glasses. *Phys. Rev. Mater.* **2019**, *3*, 015203. [[CrossRef](#)]
26. Liu, K.; Schmedake, T.A.; Tsu, R. A comparative study of colloidal silica spheres: Photonic crystals versus Bragg's law. *Phys. Lett. A* **2008**, *372*, 4517–4520. [[CrossRef](#)]
27. Wang, Y.; Cheng, W.; Qin, J.; Han, Z. Terahertz refractive index sensor based on the guided resonance in a photonic crystal slab. *Opt. Commun.* **2019**, *434*, 163–166. [[CrossRef](#)]
28. Long, J.; Xu, E.; Li, X.; Wu, Z.; Wang, F.; Xu, X.; Jin, Z.; Jiao, A.; Zhan, X. Effect of chitosan molecular weight on the formation of chitosan–pullulanase soluble complexes and their application in the immobilization of pullulanase onto Fe₃O₄-κ-carrageenan nanoparticles. *Food Chem.* **2016**, *202*, 49–58. [[CrossRef](#)]
29. Danaei, M.; Dehghankhold, M.; Ataei, S.; Hasanzadeh Davarani, F.; Javanmard, R.; Dokhani, A.; Khorasani, S.; Mozafari, M.J.P. Impact of particle size and polydispersity index on the clinical applications of lipidic nanocarrier systems. *Pharmaceutics* **2018**, *10*, 57. [[CrossRef](#)]
30. Topçu, G.; Güner, T.; Demir, M.M. Non-iridescent structural colors from uniform-sized SiO₂ colloids. *Photonics Nanostruct.-Fundam. Appl.* **2018**, *29*, 22–29. [[CrossRef](#)]
31. Arsenault, A.C.; Puzzo, D.P.; Manners, I.; Ozin, G.A. Photonic-crystal full-colour displays. *Nat. Photonics* **2007**, *1*, 468–472. [[CrossRef](#)]
32. Wang, H.; Zhang, K.Q. Photonic crystal structures with tunable structure color as colorimetric sensors. *Sensors* **2013**, *13*, 4192–4213. [[CrossRef](#)] [[PubMed](#)]
33. Gauvreau, B.; Guo, N.; Schicker, K.; Stoeffler, K.; Boismenu, F.; Aji, A.; Wingfield, R.; Dubois, C.; Skorobogatiy, M. Color-changing and color-tunable photonic bandgap fiber textiles. *Opt. Express* **2008**, *16*, 15677–15693. [[CrossRef](#)] [[PubMed](#)]
34. Smith, G.; Gentle, A.; Arnold, M.; Cortie, M.J.N. Nanophotonics-enabled smart windows, buildings and wearables. *Nanophotonics* **2016**, *5*, 55–73. [[CrossRef](#)]



© 2020 by the author. Licensee MDPI, Basel, Switzerland. This article is an open access article distributed under the terms and conditions of the Creative Commons Attribution (CC BY) license (<http://creativecommons.org/licenses/by/4.0/>).